Proton momentum distribution in solid and liquid HF

M. Krzystyniak[1,*] and T. Abdul-Redah[2]

[1]*Rutherford Appleton Laboratory, ISIS Facility, OX11 0QX Chilton, United Kingdom*
[2]*Institute of Chemistry, Technical University of Berlin, Str. d. 17. Juni 135, D-10623 Berlin, Germany*

Neutron Compton scattering (NCS) experiments were performed on liquid and solid HF, a system where the effective Born-Oppenheimer (BO) potential energy surface is not isotropic. Proton momentum distributions were calculated in the framework of the impulse approximation from measured neutron Compton profiles. A detailed data analysis shows that there are no systematic changes in the width, position of the maximum, or excess kurtosis of proton momentum distributions in both systems with increasing scattering angle. This observation has important implications for further theoretical work on violation of BO approximation in the presence of ultrafast neutron-proton scattering. That is, the picture of proton dynamics in HF emerging from the analysis of NCS data does not seem to support the previously considered model of protons accessing excited electronic states due to ultrafast scattering.

PACS number(s): 03.65.Yz, 03.65.Nk, 34.90.+q

I. INTRODUCTION

Neutron Compton scattering (NCS) is a unique technique that can be applied to investigate the momentum distribution of the proton reflecting its ultrafast dynamics in condensed matter.[1–3]

In recent theoretical works on neutron scattering[4,5] it has been proposed that an ultrafast neutron-proton scattering process may induce changes in the proton momentum distribution due to changes in the Born-Oppenheimer approximation (BOA). Motivated by these theoretical models, Krzystyniak *et al.*[6] preformed a detailed analysis of proton momentum distributions measured by NCS in the pseudospherical ammonium ion in ammonium hexachloropalladate and ammonium hexachlorotellurate. No systematic broadening or distortion of proton momentum distribution was observed in both systems and the measured proton kinetic energies corresponded to values obtained from *ab initio* calculations. The analysis led to the hypothesis that the high symmetry of the effective potential experienced by the protons leads to an unperturbed proton momentum distribution. In this context, a very interesting question has emerged, i.e., whether the presence of anisotropy in the effective BO potential may lead to a distortion of the proton momentum distribution. This was the motivation for the NCS work presented here.

The theoretical works[4,5] mentioned above belong to a series of further theoretical models[7–11] aiming at explaining a striking anomalous deficit of neutron-scattering intensity observed in experiments on hydrogen-containing materials.[4,5,7–20] Although neither the experimentally observed intensity deficit nor its theoretical explanation is the main subject of the present work, it should be mentioned here that, to date, no agreement has been reached upon the genuineness of the intensity deficit or taking it as a genuine physical effect upon which of the existing theoretical models gives a satisfactory account of all its features. And it is not the intention of the present work to contribute to this dispute. For some discussions, see[2,21–24] and the references therein.

HF seems to be a very interesting system as far as the investigation of the applicability of the effective BO potential for the description of proton dynamics is concerned. First of all, HF is the archetype for a strong hydrogen bond due to its molecular simplicity.[25–28] The hydrogen bond is the dominant feature of the structural chemistry of HF in all phases; the solid is composed of unbranched, zigzag chains[29] while the vapor is composed of cyclic oligomers and clusters.[30] In the liquid, the macroscopic properties are consistent with strong hydrogen bonds, which has been confirmed at the pair correlation function level from neutron diffraction.[25] Due to the directionality of the H bond, protons in HF, both in the liquid and solid state, exhibit an anisotropic effective Born-Oppenheimer potential. Second, and most importantly in the context of the theoretical models mentioned above, HF has been a subject of numerous theoretical studies as far as the failure of the Born-Oppenheimer approximation for describing the proton dynamics is concerned.[31–35] Mills[31] considered changes in the effective potential function of a low-frequency large-amplitude molecular vibration in a HF dimer, resulting from excitation of a high-frequency vibration. It was shown that in some situations a significant contribution to such changes may arise from the failure of the Born-Oppenheimer separation of the low-frequency mode. Pine and co-workers[35] observed, in high-resolution spectra of the intermolecular stretching bands of $(HF)_2$, the vibrational predissociation of the HF dimer when one of the monomers was excited and attributed this effect to the breakdown of the BOA.

In NCS work presented here, proton momentum distribution has been measured in liquid and solid HF as a function of momentum and energy transfer from impinging neutron probes. An advanced data reduction scheme has been applied that extracts the proton momentum distribution from measured NCS time-of-flight (TOF) spectra in a model-free manner using Gram-Charlier expansion (GCE).[3,36] The data treatment from NCS experiments by means of GCE yields no broadening, nor a shift of the maximum, or a change in excess kurtosis of proton momentum distribution with increasing scattering angle. Together with previous results from NCS work on ammonium hexachlorometallates,[6] the present result shows that no observable distortion of the proton momentum distribution is present during an ultrafast neutron-

proton collision no matter whether the proton experiences isotropic or anisotropic BO potential. This result has interesting implications for further theoretical investigation of proton momentum distribution in condensed matter systems and molecules by means of neutron Compton scattering.

The paper is organized as follows. In Sec. II the theory of NCS in the presence of impulse approximation (IA) is introduced. In Sec. III the new setup of the NCS spectrometer Vesuvio at the ISIS neutron spallation source is briefly described. Section IV presents details of data treatment to obtain nuclear momentum distribution from NCS spectra. Finally, general implications of the obtained results for future theoretical work on neutron Compton scattering are discussed.

II. NCS SCATTERING INTENSITIES IN IMPULSE APPROXIMATION

In what follows only a brief description will be given. For a recent rigorous theoretical treatment of neutron Compton scattering refer to work by Mayers *et al.*[37] or recent review by Andreani *et al.*[3] In NCS the energy and momentum transfers from the neutron to the scattering nuclei are so high that the scattering process can be treated within the IA limit.[1,38–42] In the IA limit, i.e., in the limit of infinite momentum transfer q, the scattering function $S(q,\omega)$ reduces to a single peak centered at the recoil energy $\omega_r = q^2/2M$ of the corresponding nucleus of mass M, i.e., $S(q,\omega) = M/qJ(y)$, where y is the momentum p of the nucleus in the initial state projected onto the scattering vector q (Refs. 38 and 43)

$$y = \mathbf{p} \cdot \hat{\mathbf{q}} = (M/q)(\omega - \omega_{\mathbf{r}}) = (M/q)(\omega - \mathbf{q}^2/2M), \quad (1)$$

where $\hat{\mathbf{q}}$ is the unit vector in the direction of the momentum transfer. $J(y)$ is the so-called Compton profile[1,38] representing the momentum distribution of the scattering nucleus along y. For a harmonically bound isotropic system, in which $n(\mathbf{p})$ depends only on the magnitude of $\mathbf{p}$, $p = |\mathbf{p}|$, $J(y)$ in the IA limit is most commonly written as a normalized Gaussian form[3,37,39,42,44]

$$J_{\mathrm{IA}}(y) = \frac{1}{\sqrt{2\pi\sigma_p^2}}\exp\left(\frac{-y^2}{2\sigma_p^2}\right) \quad (2)$$

with standard deviation σ_p.

The corrections to the IA for the finite q of measurement, known as "final states effects" (FSE), have been extensively discussed in recent reviews by Mayers *et al.*[37] and Andreani *et al.*[3] From different approaches on how to account for FSE in NCS the method of Sears[38] is routinely incorporated in standard NCS data treatment.[37] Sears showed that the effects of finite transfers of momentum and energy, q and ω, can be accounted for by expressing the neutron Compton profile $J(y)$ as

$$J(y) = J_{\mathrm{IA}}(y) - \frac{M\langle\nabla^2 V\rangle}{36\hbar^2 q}\frac{d^3}{dy^3}J_{\mathrm{IA}}(y) + \cdots, \quad (3)$$

where $J_{\mathrm{IA}}(y)$ is the IA result. $\langle\nabla^2 V\rangle$ is the mean value of the Laplacian of the potential energy of the atom.[37]

For a real experimental situation the total number of neutrons detected for a given mass M in a time channel t is
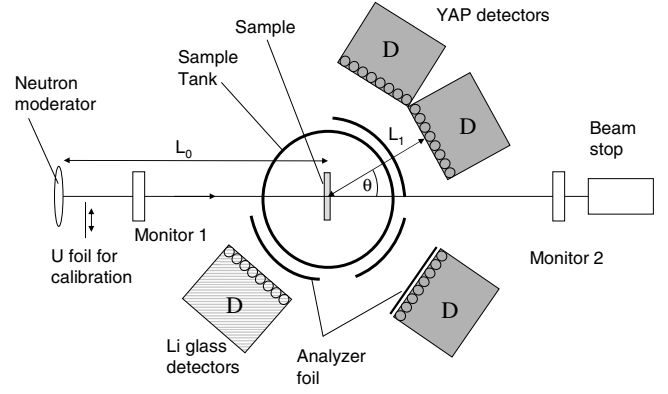

FIG. 1. A schematic representation of the Vesuvio spectrometer at ISIS.

proportional to the Compton profile, $J(y_M)$, convoluted in the y_M space with the mass-dependent instrument resolution function $R(y_M)$. Thus, for N different masses present in the sample the total count rate at a fixed scattering angle θ, $C_\theta(t)$ is (Ref. 37, Eq. 2.22)

$$C_\theta(t) = A'\left[\frac{E_0 I(E_0)}{q}\right]_t,$$

$$\sum_{n=1}^{N} I_n M_n J_n[y_n(t)] \otimes R_n[y_n(t)], \quad (4)$$

where A' is a mass-independent experimental constant and the mass-independent factor $\left[\frac{E_0 I(E_0)}{q}\right]_t$ depends on the spectrum, $I[E_0(t)]$, the initial neutron energy, $E_0(t)$, and the momentum transfer $q(t)$, all being functions of time of flight t (Ref. 37). In Eq. (4) the nuclear momentum distribution of the mass M, $J_M[y_M(t)]$, is given by the formula (3).

III. VESUVIO NCS SPECTROMETER AT ISIS SPALLATION SOURCE

The NCS spectrometer Vesuvio at the ISIS neutron spallation source is an inverted geometry time-of-flight instrument.[37] The sample is exposed to a polychromatic neutron beam characterized by the incident neutron energy spectrum $I(E_0)$. Incident neutrons having initial energy E_0 travel a distance L_0 from the pulsed source to the sample. After scattering at an angle θ, neutrons of final energy E_1 travel a distance L_1 to the detector position (Fig. 1).

The TOF spectrum in forward scattering is obtained in the following way: a thin gold foil is placed in front of the detector. This foil absorbs neutrons at $E_1 = 4.9$ eV in a narrow range of energy, by which the final energy of the scattered neutron is determined. In order to enhance the energy resolution of the instrument a second foil is cycled in and out of the scattered neutron beam. By taking the difference of both spectra one obtains the final TOF spectrum, which then is subject to data reduction and analysis. The TOF spectrum in the backscattering direction is obtained by taking the difference of two spectra: one with the gold foil between the sample and the detector and one without a foil.

The detector material in forward scattering is different from that in backscattering. While the forward-scattering detectors consist of yttrium aluminum perovskite (YAP) crystals and detect the γ rays emitted by the gold nuclei after neutron capture, the backscattering detectors consist of glass doped with Li and are sensitive to neutrons only. The detection principles and the implications for the energy resolution are described in detail by Imberti *et al.*[45]

IV. NUCLEAR MOMENTUM DISTRIBUTION FROM NCS MEASUREMENT

In an NCS experiment performed on an isotropic sample, a longitudinal momentum distribution, $J(y)$, of a spherically averaged three-dimensional momentum distribution, $n(p)$, is measured, where[3,36]

$$n(p) = \frac{-1}{2\pi y} \left. \frac{\partial J(y)}{\partial y} \right|_{y=p}. \quad (5)$$

In the case of rhombic symmetry, where the radial nuclear momentum distribution, $n(p)$, is characterized only by two variances $\sigma_x^2 = \sigma_y^2 = \sigma_t^2$ and σ_z^2, the spherical average of $n(p)$ (denoted here as $\langle \cdots \rangle_\Omega$)

$$n(p) = \left\langle \frac{1}{\sigma_t^2 \sigma_z \sqrt{8\pi^3}} \exp\left[-1/2 \left(\frac{p_z^2}{\sigma_z^2} + \frac{p_t^2}{\sigma_t^2} \right) \right] \right\rangle_\Omega \quad (6)$$

can be represented as[3,36]

$$n(p) = \frac{\exp\left(\frac{-p^2}{2\sigma^2} \right)}{(\sigma\sqrt{2\pi})^3} \sum_n c_n (-1)^n L_n^{1/2} \left(\frac{p^2}{2\sigma^2} \right), \quad (7)$$

where $L_n^{1/2}$ denotes generalized Laguerre polynomials.

Equation (7) can be used for the reconstruction of the radial momentum distribution profile from the measured Compton profile fitted with the Gramm-Charlier expansion[3,36] for the longitudinal momentum distribution, $J(y)$

$$J(y) = \frac{\exp\left(\frac{-y^2}{2\sigma^2} \right)}{(\sigma\sqrt{2\pi})} \sum_n \frac{c_n}{2^{2n} n!} H_{2n} \left(\frac{y}{\sigma\sqrt{2}} \right), \quad (8)$$

where H_{2n} denotes Hermite polynomials.

In the above expression, the coefficients c_n are identical with the expansion coefficients in expression (7) for the radial momentum distribution given above, which is tantamount to the inversion procedure between $J(y)$ and $n(p)$.[5]

In order to compare the results of the *ab initio* momentum distribution calculation presented above with the experimental results obtained from NCS measurements the following protocol was applied to reduce the entire TOF spectra. (1) The entire TOF spectrum, containing multiple recoil peaks from different masses M, was fitted directly in TOF with the function $C(t)$ being a combination of the Gram-Charlier expansion for protons, J_H, and the sum of Gaussian momentum distribution functions for $M \neq M_H$, J_M, both convoluted with the mass-dependent resolution functions, R_M.[3,36] In the

Gram-Charlier expansion, the only statistically significant member was the coefficient c_4. This situation is encountered very often in fitting NCS spectra and reflects the present accuracy of Vesuvio.[3,36,46] Additionally, FSE contributions to both Gaussian and non-Gaussian J_M are accounted for by including terms proportional to $1/qH_3$. The resulting expression to fit the entire TOF spectrum is of the following form:

$$C(\theta = const, t) = A' \frac{E_0 I[E_0]}{q} \left[J_H(x_H) \otimes R_H(x_H) \right.$$
$$\left. + \sum_{M \neq M_H} J_M(x_M) \otimes R_M(x_M) \right], \quad (9)$$

where

$$J_H(x_H) = \frac{\exp(-x_H^2)}{\sqrt{2\pi\sigma_H^2}} \left(1 + \frac{c_4}{32} H_4(x_H) - \frac{k}{q} H_3(x_H) \right) \quad (10)$$

and

$$J_M(x_M) = \frac{\exp(-x_M^2)}{\sqrt{2\pi\sigma_M^2}} \left(1 - \frac{k}{q} H_3(x_M) \right) \quad (11)$$

with $x_M = [y_M - y_0(M)]/[\sigma(M)\sqrt{2}]$ where $y_0(M)$ is the shift of the position of the maximum of a nuclear momentum distribution from the center of the recoil line and $\sigma(M)$ is the standard deviation of the momentum distribution for a mass M. FSE expansion in the limit of a harmonic potential leads to a very useful expression of the FSE coefficient k in the expansion given by Eq. (9), $k = \sigma\sqrt{2}/12$. Thus, fitting the magnitude of the FSE and comparing it with the theoretical expression provides a very useful check of the harmonic approximation. (2) The widths of the nuclear momentum distribution of fluorine, $\sigma(F)$, were fixed in fitting. $\sigma(F)$ was set to the value obtained from the theory of quantum mechanical harmonic oscillator, which is a common practice in many NCS studies of condensed matter systems and molecules.[3] The quantum mechanical prediction yielded $\sigma(F) = 16.26$ Å^{-1}, for the tabulated value of HF vibrational mode of 4138.32 cm^{-1} (Ref. [47]). (3) As in all TOF spectra recorded on Vesuvio, the fluorine recoil peak overlaps with the recoil peak of the Monel can used as a sample container. A feasible procedure had to be adopted for modeling the Monel can momentum distribution. A Gaussian momentum distribution was assumed with the standard deviation calculated from the Debye solid model using the literature value of Debye temperature for Monel alloy $\Theta_{Monel} = 475$ K.[48,49] This value of Debye temperature gives the standard deviations of $\sigma(Monel)$ equal to 17.1 and 20 Å^{-1}, at 180 K and 290 K, respectively. These values were fixed in fitting. The time of flight position of the recoil peak due to Monel was determined using the effective average mass of Monel. The effective mass was calculated taking the bound neutron scattering cross sections of metals composing the Monel alloy as statistical weights. The specification of the used Monel is 34% Cu and 66% Ni. Their bound scattering cross sections were taken as 8.03 and 18.5 barn, respectively.[50] Thus, the effective mass, $M_{Monel} = [0.34 \times 63.55 \times 8.03 + 0.66 \times 58.69 \times 18.5]/[0.34 \times 8.03 + 0.66 \times 18.5] = 59.6$ amu. (4) Additionally, for

all nuclei other than protons the shifts $y_0(M)$ of the Compton profiles from the centers of the recoil lines for masses M were fixed to $y_0(M)=0$ in the fitting procedure. Thus, the free fitting parameters were: the proton recoil peak shift $y_0(H)$, the standard deviation of the proton momentum distribution $\sigma(H)$, the magnitude of FSE, $k(H)$, and the values of $c_4(H)$. It turns out that in the Gram-Charlier expansion $c_4=\delta/3$, where δ is the excess kurtosis of the single-particle momentum distribution, $\delta=(\mu_4-3\langle\sigma^2\rangle^2)/\langle\sigma^2\rangle^2$, with μ_4 being the fourth moment of the momentum distribution.[36,51] (5) A sequential fit was performed of $\sigma(H)$, $c_4(H)$, $k(H)$, and $y_0(H)$ detector by detector in the forward-scattering range. (6) A weighted average of $\sigma(H)$, $c_4(H)$, $k(H)$, and $y_0(H)$ was performed over a selected range of detectors. This selected range corresponded to detectors placed at scattering angles above 40° and below 70°. For scattering angles lower than 30°, the proton recoil peaks may overlap with the recoil peaks of F and Monel. For scattering angles higher than 70°, the proton recoil peaks are disturbed by instrument background at short time of flight values. In both cases, the full analysis of the recorded shape of proton momentum distribution could possibly suffer from artifacts.

Figures 2 and 3 show the widths, $\sigma(H)$, the shifts of the momentum distribution peak of protons, $y_0(H)$, the Gram-Charlier expansion coefficients, $c_4(H)$, and the magnitude of FSE, $k(H)$, obtained of proton momentum distribution in solid and liquid HF at 180 K and 290 K, respectively. Table I lists weighed averages, over the whole set of forward-scattering detectors, of $\sigma(H)$, $y_0(H)$, $c_4(H)$, and $k(H)$. The overall fitting statistics, in terms of reduced chi square values, was at the level of 1.04 and 1.08, for HF at 180 K and 290 K, respectively. The fitted value of the proton momentum distribution width, $\sigma(H)$ at 290 K is 4.8 ± 0.1. At 180 K the fitted value of $\sigma(H)$ is 4.5 ± 0.1. The same trend as for $\sigma(H)$ is observed for the magnitude of FSE: no tendency whatsoever has been observed with increasing scattering angle. For both, $\sigma(H)$ and $k(H)$, the overall accuracy is satisfactory (the standard deviation is at the level of 2% of their respective mean values). A bit larger scatter of data is present in both samples for the fitted values of $c_4(H)$. The standard deviations of $c_4(H)$ are at the level of 14%. Most importantly, however, the magnitude of errors $\sigma(H)$, $k(H)$, and $c_4(H)$ is typical for results of proton momentum distribution analysis in NCS at present level of the accuracy of the technique.[3] The biggest scatter of data is present for the fitted values of the shifts of the centers of proton momentum distributions, $y_0(H)$. The standard deviations of $y_0(H)$ are equal to 0.2 Å^{-1} for both HF at 180 and 290 K. Most importantly, also here no tendencies have been observed for the magnitudes of the shifts with increasing scattering angles.

Comparison of fits of the longitudinal, $J(y)$, and radial, $4\pi p^2 n(p)$, momentum distributions to the HF liquid and solid data are shown in Figs. 4 and 5, for HF at $T=180$ K and $T=290$ K, respectively. Both distributions are plotted using average the values given in Table I. In the longitudinal momentum distribution functions $J(y)$, FSE were included through the Sears expansion and simulated in the plotted curves for the magnitude of the momentum transfer $q=45$ Å^{-1}. In the radial momentum distributions the FSE contribution to the simulated curves is omitted.
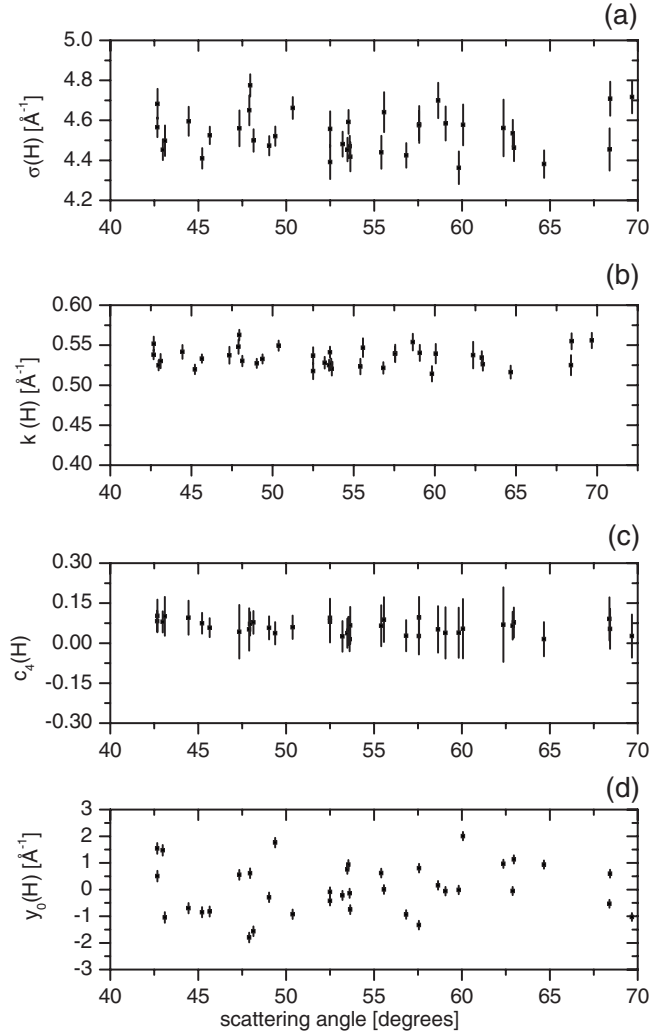

FIG. 2. Results of the fitting Gram-Charlier expansions to the proton Compton profiles recorded in HF at 180 K. (a) $\sigma(H)$ values, (b) the FSE magnitude, $k(H)$, (c) the values of $c_4(H)$ coefficients, and (d) the shifts in the positions of recoil peak centers, $y_0(H)$.

Inspection of the results presented in Figs. 2 and 3 shows that no systematic increase in the widths, the magnitude of the final states effects, the excess kurtosis of momentum distributions or of the recoil peak position in y space is observed in both HF samples with increasing scattering angle.

The Watson-scattering time,[1] calculated for standard deviation of proton momentum distribution $\sigma(H)=4.7$ Å^{-1}, is equal to approximately. 1.17 fs at the scattering angle of 30° and to approximately 0.32 fs at 60°.[52] Thus, any increase in the value of standard deviation, the magnitude of FSE, and/or excess kurtosis with increasing scattering angle would point at possible effects of the scattering process taking place at shorter times on the proton momentum distribution. Thus, the main result of the analysis of proton momentum distributions in solid and liquid HF is that no extra broadening is present that would have been due to ultrafast kinetics of the scattering process postulated in the literature.[4,5,7]

V. DISCUSSION

The major goal of the NCS work presented here was to categorize the proton momentum distribution in liquid and
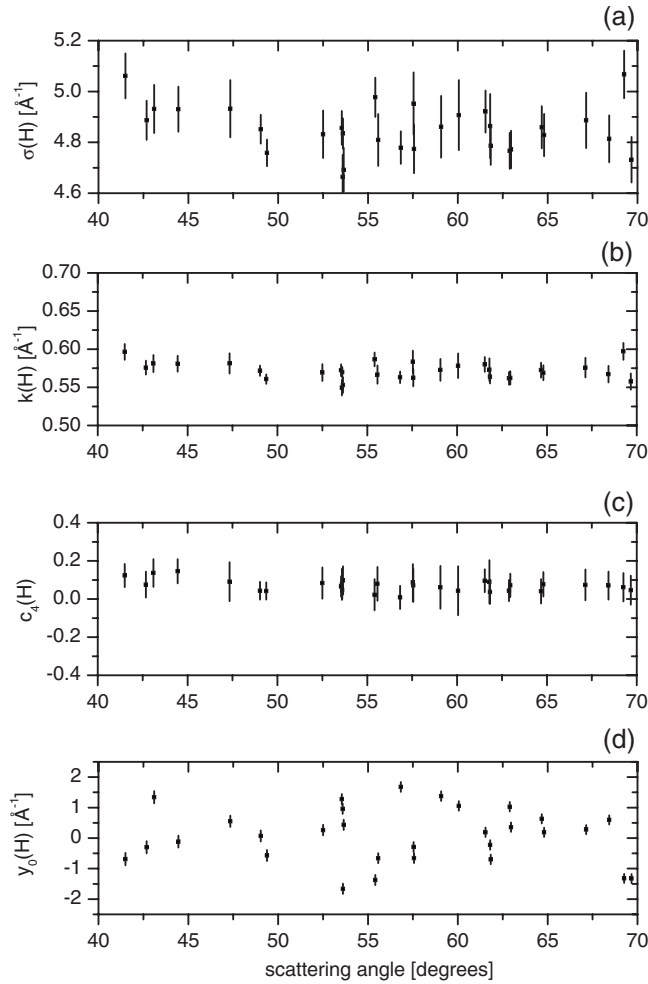
FIG. 3. Results of the fitting Gram-Charlier expansions to proton Compton profiles recorded in HF at 290 K. (a) $\sigma(H)$ values, (b) the FSE magnitude, $k(H)$, (c) the values of $c_4(H)$ coefficients, and (d) the shifts in the positions of recoil peak centers, $y_0(H)$.

solid HF as a function of kinematic variables, i.e., scattering angle, energy and momentum transfer at the center of the proton recoil peak. This was achieved employing the Gramm-Charlier expansion. The Gramm-Charlier expansion, being model free, takes into account all effects leading to a non-Gaussian shape of the momentum distribution. These effects may be related to spherical averaging of the multivariate three-dimensional-Gaussian distribution but also can

TABLE I. The widths, $\sigma(H)$, the shifts of the momentum distribution peak centers, $y_0(H)$, the Gram-Charlier expansion coefficients, $c_4(H)$, and the magnitude of FSE, $k(H)$, obtained by fitting recorded proton momentum distributions in solid and liquid HF at 180 K and 290 K, respectively. All values are weighed averages over the whole set of forward-scattering detectors.

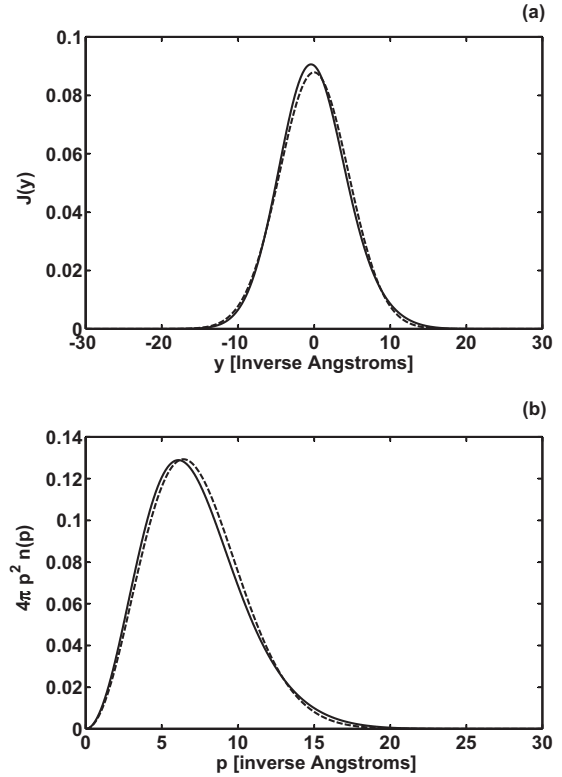| T (K)	$\sigma(H)$ (Å^{-1})	$y_0(H)$ (Å^{-1})	$c_4(H)$	$k(H)$ (Å^{-1})
180	4.5 ± 0.1	0.1 ± 0.2	0.07 ± 0.01	0.53 ± 0.01
290	4.8 ± 0.1	0.0 ± 0.2	0.08 ± 0.01	0.56 ± 0.01

FIG. 4. Longitudinal, $J(y)$, and radial, $4\pi p^2 n(p)$, momentum distributions for HF at $T = 180$ K. The functions $J(y)$ and $n(p)$ are plotted for the average values of standard deviation of momentum distributions $\sigma(H)$ and Gram-Charlier expansion coefficients $c_4(H)$ given in Table I. In the longitudinal momentum distribution functions $J(y)$, FSE were included through the Sears expansion and simulated in the plotted curves for the magnitude of the momentum transfer $q = 45$ Å^{-1}. In the radial momentum distributions the FSE contribution to the simulated curves is omitted. The dashed lines represent momentum distributions calculated in absence of nonharmonic contributions, i.e., with excess kurtosis set to zero and other moments of the Gram-Charlier expansion unchanged.

result from an anharmonicity in the local effective potential felt by the proton in any direction in space.

The second moment of the proton momentum distribution calculated from experimental data of liquid HF at 290 K and for the orthorhombic HF crystal at 180 K is independent of the scattering angle. Due to the fact that the Gramm-Charlier series is orthogonal and complete, this observation is independent of the extent of the anharmonicity of the local effective potential experienced by the protons.

Nonvanishing excess kurtosis is responsible for a redistribution of the proton momentum distribution to higher momentum values. Values of excess kurtosis around 0.2 have already been obtained for supercritical water at normal conditions.[53,54] Slightly higher values, approximately 0.3, have been obtained for ice I_h and ice VI.[55] In both cases a redistribution in proton momentum distribution was interpreted as the result of binding of the proton to its covalently bonded atom.[55,56] The proton momentum distribution can be thought of as arising from its confinement in the potential well provided by covalently bonded neighbor atom, which can be regarded as fixed in position in the time scale of
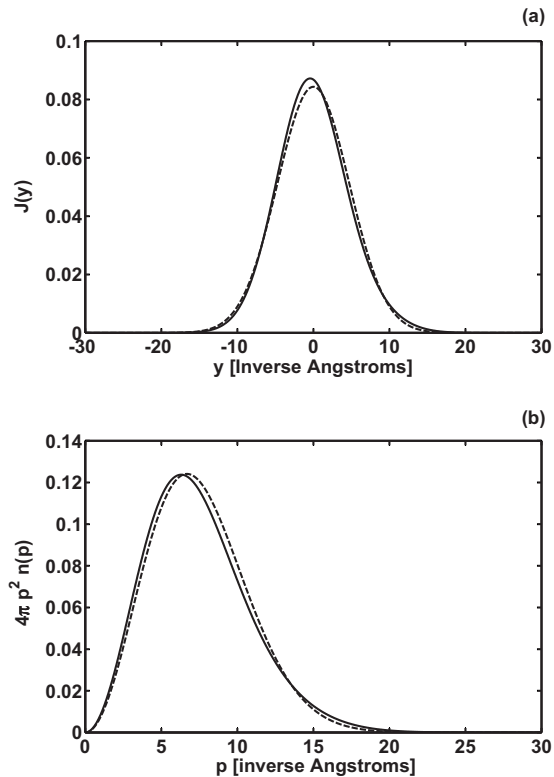
FIG. 5. Longitudinal, $J(y)$ and radial, $4\pi p^2 n(p)$, momentum distributions for HF at $T=290$ K. The functions $J(y)$ and $n(p)$ are plotted for the average values of standard deviation of momentum distributions $\sigma(H)$ and Gram-Charlier expansion coefficients $c_4(H)$ given in Table I. In the longitudinal momentum distribution functions $J(y)$, FSE were included through the Sears expansion and simulated in the plotted curves for the magnitude of the momentum transfer $q=45$ Å^{-1}. In the radial momentum distributions the FSE contribution to the simulated curves is omitted. The dashed lines represent momentum distributions calculated in absence of nonharmonic contributions, i.e., with excess kurtosis set to zero and other moments of the Gram-Charlier expansion unchanged.

proton motion. Thus, the effect of fluorine atoms on the protons momentum distribution cannot be really though of as arising from a static potential. The F atoms in HF provide thus a single-particle effective potential.[53] The excess kurtosis fitted to Compton profiles recorded in both liquid and solid HF is around 0.07 (see Table I). For the values of 0.07 the inversion procedure of the momentum distribution function leads to a single-well potential. Thus, the effects of intermolecular hydrogen bonds in HF do not seem to manifest themselves markedly in the measured proton momentum distribution. This results in a situation where no tunnelling across the H bonds is a realistic option but rather a slightly distorted non-Gaussian proton momentum distribution across the bond. This is further reinforced by observing that the fitted magnitude of final states effects, k, in both samples of interest is very well reproduced by an average harmonic potential corresponding to the average measured widths of momentum distribution (i.e., the relation $k=\sigma\sqrt{2}/12$ is very well fulfilled). This picture seems to be supported by the fact that, as shown in the literature, a certain amount of anharmonicity of the effective potential of the protons in hydrogen-bonded

HF molecules is needed to account for the results of the vibrational spectroscopy on HF.[57,58] In the presence of H bond, the H-F bond stretch gets redshifted.[57] Moreover, the *ab initio* calculation of a cluster of HF molecules at the MP2 level including anharmonic effects shows strong dependence of computed intramolecular frequencies on cluster size, also reporting redshifted spectra for HF trimers and tetramers.[58]

The second aim of the presented work was to test recent theoretical predictions about the possible distortion of the shape of the proton momentum distribution in condensed matter systems in the presence of ultrafast proton-neutron collision in NCS. The constancy of the observed parameters of the proton momentum distribution in both liquid and solid HF—the standard deviation of proton momentum distribution, the excess kurtosis of the distribution, the recoil peak position, and the magnitude of the final states effects leads to the conclusion that there is no extra broadening or peak shift of the proton momentum distribution due to ultrafast kinetics of Compton scattering in both systems. This experimental result has important consequences for theoretical models describing NCS scattering process in terms of non-Born-Oppenheimer proton dynamics in the final state.[4,5,7]

The model by Reiter and Platzman[4,5] postulates the breakdown of the BOA in the final state of the scattering process which contains a very rapidly moving proton with sufficient energy to mix the electronic states of the system.[5] The theory predicts, in the weak-coupling region, the buildup of additional recoil peaks being replicas of the main Compton profile. These additional recoil peaks would be shifted toward high energy transfers (short time-of-flight values) by the amounts of energy equal to the energy level difference between the ground and subsequent excited molecular electronic levels. The net observable result of the proposed ultrafast neutron-proton scattering scenario would be the redistribution of NCS scattering intensity and in the same time the shift of the center of gravity of the main recoil peak toward low-energy transfers (long time-of-flight values) due to the conservation of the first-order sum rule in neutron scattering.[5] Moreover, in some cases, in order to account for results of NCS studies on some molecular systems (e.g., water and metal hydrides) the theory allows for an intermediate coupling regime in which no net shift of the main recoil peak can be observed within the angular resolution of the NCS technique in its present incarnation.[3] Instead, a broad and wide background should be present in recorded NCS spectra.[5] Also, in the model by Gidopoulos[4] a broadening accompanied with the shift of the main recoil peak is expected if one goes beyond the simplest case of a two-level electronic system accessed by the proton in the final state of the collision. From the data treatment point of view, the broadening resulting from both theoretical models would manifest itself in effectively observed NCS spectra in three possible ways: (i) an increase in the width of proton momentum distribution with increasing scattering angle, (ii) an increase in the nonharmonic contribution to the proton recoil line shape with increasing scattering angle, and/or (iii) a broad slowly varying background in TOF. The contributions of type (i) and type (ii) have not been detected as there is no visible trend in the values of the second moment and the excess kurtosis of momentum distributions in both systems

as a function of the scattering angle. The contribution of type (iii) cannot be entirely excluded as all forward-scattering spectra recorded did contain some broad background that was accounted for by fitting third order polynomial functions in TOF. Ideally, such broad background would persist for all forward-scattering angles. Unfortunately, the TOF background on Vesuvio changes from detector to detector, making the assessment about any systematic contributions impossible.

A different scenario of the violation of BOA due to ultrafast neutron-proton scattering is encountered in the model put forward by Kurizki, Mazets, and Chatzidimitriou-Dreismann.[7] In this model a neutron impinges on a target, which is described to be composed of the nucleus and of electrons coupled to environmental electronic degrees of freedom, the coupling strength of which is given by a momentum transfer-dependent relaxation rate.[7] The inclusion of fast environmentally induced relaxation in the theoretical description of the neutron Compton scattering leads to a generalized (skewed) Lorentzian line shape of the final (target and projectile) state induced by the environment. If the spread of the nuclear momentum distribution in the initial state of the target nucleus is much larger than that of the line shape of the final state, no extra broadening of proton momentum distribution is observed. However, in case of a very large relaxation rate the theory predicts an extra broadening of the proton recoil peak beyond that of the initial state momentum distribution.[7] If the model by Kurizki *et al.* still applies in case of NCS scattering, it would require weak or intermediate coupling in the entire energy transfer domain accessible (from 3 eV at the scattering angle of 30° up to 40 eV at the scattering angle of 70°).

On the whole, in the context of the results of present and other recent NCS experiments aiming at discovering a possible distortion of the momentum distribution of the proton due to ultrafast neutron-proton collision, the effect, if present, seems to manifest itself in a more subtle way than originally anticipated. One possible reason for such behavior is the present experimental setup, namely, the so-called constant- scattering angle instrument trajectories used to record NCS spectra. The usual theoretical treatment of the neutron-proton collision in the composite projectile-target system assumes entirely different experimental regime. Namely, it is assumed, either explicitly[7] or implicitly,[4,5] that the scattering is at constant magnitude or direction of the momentum transfer vector. In the experiments on HF described here, both liquid and solid samples were not oriented. The proton recoil peak in a TOF spectrum is wide enough for the magnitude of the incident neutron wave vector, k_0, to change appreciably across the peak. As a result of this, the angle between the incident neutron wave vector and the momentum transfer direction, $\hat{q}$, also changes considerably across the recoil peak. Thus, NCS spectra on isotropic samples contain information about the spatial average of the multidimensional nuclear momentum distribution. Such averaging may lead to masking the differences in shapes of momentum distribution along different q directions. The ideal experimental test of theoretical predictions discussed above would, therefore, require specially designed NCS experiments.

The main result that should motivate further theoretical work on the possibility of the violation of BOA in NCS is the question about the limits of the weak and strong coupling regimes in the models by Reiter and Platzman, and Kurizki and Chatzidimitriou-Dreismann, respectively. It is very difficult if not impossible to discern concrete quantitative predictions for such limits from the present models. The chief difficulty in the model by Reiter and Platzman is the lack of numerical estimates for expectation values of perturbation between relevant excited electronic states.[4,5] One quantitative prediction that can be made is based on the simplified two-level model by Gidopoulos[4] in which the coupling strength is proportional to the square root of the initial kinetic energy of the target proton which in turn is proportional the spread of the proton wave function after collision (see Eq. 14 in Ref. [4]). Neglecting the rotational and translational degrees of freedom, which is a very good approximation for proton kinetic energy even at room temperature,[3] the coupling limit is proportional to the square root of the vibrational kinetic energy of the struck proton. In such case, HF constitutes one of the best systems to test the strong regime of the model by Gidopoulos as the stretching mode energy in HF, being around 0.5 eV, is one of the highest vibrational mode energies encountered in molecular systems.[47] However, from the present experimental evidence it seems plausible to conclude that, HF as well as many other systems investigated so far are likely to lie in the weak coupling limit. Thus, in order for the above mentioned theoretical models to satisfactorily account for the violation of the BOA in NCS it seems that the models must: (i) take into account mixing of the ground with more than just one excited electronic wave functions and (ii) predict transition between the weak and strong coupling regime at very high momentum and energy transfers from neutrons, perhaps even beyond the kinematic values experimentally obtainable by the NCS technique at present.

Most importantly for the presented work, the issue of the violation of BOA in NCS arises solely from the ultrafast kinetics of the neutron-proton collision and as such can be discussed in its own right. It is insofar completely independent on the possibility of existence of the anomaly of the scattering cross-section density for protons in condensed matter and molecules, although the theoretical models discussing the non-BOA effects in neutron Compton scattering were motivated by the reported anomaly.

VI. CONCLUSIONS

Proton momentum distribution has been measured by neutron Compton scattering in liquid and solid HF at 180 K and 290 K, respectively. The spherically averaged multivariate three dimensional nuclear momentum distribution was characterized by fitting the recorded Compton profiles with the model-free Gram-Charlier expansion.

The fitting of the expansion to recorded neutron Compton spectra has not resulted in large values of excess kurtosis of proton momentum distributions. Thus, the anharmonicity of local effective potential felt by protons in solid and liquid HF does not seem to manifest itself in neutron Compton profiles

under realistic experimental conditions. Clearly, further NCS experiments and more elaborate theoretical models are still needed to fully understand the proton dynamics in strongly hydrogen-bonded systems such as HF.

The shape of the proton momentum distribution, in both liquid and solid HF, has been constant over the whole range of scattering angles (the whole range of scattering times). This is an important experimental result as it has consequences for proposed theoretical models postulating systematic distortions of the proton momentum distribution due to ultrafast proton-neutron collision in the Compton scattering regime. Thus, at least for the system under consideration and within present experimental accuracy, the proposed mechanism[4,5] of the violation of the Born-Oppenheimer approximation does not seem to account for the observed nuclear Compton profiles. For the test of theoretical models based on the violation of the Born-Oppenheimer approximation, specially designed NCS experiments are in demand with extremely good counting statistics and minimal contribution from the experimental background.

As far as theoretical predictions of the proton momentum distribution in NCS involving decoherence mechanisms are concerned,[2,7,8] the present experiment has not given a conclusive answer whether such models are applicable. Here also specially designed NCS experiments are in demand in the future with samples oriented in the neutron beam. In such experiments, full advantage can be taken from the ability of the instrument to selectively measure Compton profiles along specific directions in momentum space.

ACKNOWLEDGMENTS

*matthew.krzystyniak@stfc.ac.uk

[1] G. I. Watson, J. Phys.: Condens. Matter **8**, 5955 (1996).

[2] C. A. Chatzidimitriou-Dreismann and M. Krzystyniak, Laser Phys. **20**, 990 (2010).

[3] C. Andreani, D. Colognesi, J. Mayers, G. F. Reiter, and R. Senesi, Adv. Phys. **54**, 377 (2005).

[4] N. I. Gidopoulos, Phys. Rev. B **71**, 054106 (2005).

[5] G. F. Reiter and P. M. Platzman, Phys. Rev. B **71**, 054107 (2005).

[6] M. Krzystyniak, Z. T. Lalowicz, C. A. Chatzidimitriou-Dreismann, and M. Lerch, J. Phys.: Condens. Matter **21**, 075502 (2009).

[7] I. E. Mazets, C. A. Chatzidimitriou-Dreismann, and G. Kurizki, in *Decoherence, Entanglement and Information Protection in Complex Quantum Systems*, edited by V. M. Akulin, A. Sarfati, G. Kurizki, and S. Pellegrin (Springer, Dordrecht, 2005), Vol. 549.

[8] C. A. Chatzidimitriou-Dreismann and S. Stenholm, in *Decoherence, Entanglement and Information Protection in Complex Quantum Systems*, edited by V. M. Akulin, A. Sarfati, G. Kurizki, and S. Pellegrin (Springer, Dordrecht, 2005), Vol. 555.

[9] E. B. Karlsson and S. W. Lovesey, Phys. Rev. A **61**, 062714 (2000).

[10] E. B. Karlsson and S. W. Lovesey, Phys. Scr. **65**, 112 (2002).

[11] E. B. Karlsson, Phys. Scr. **77**, 065301 (2008).

[12] C. A. Chatzidimitriou-Dreismann, T. Abdul Redah, R. M. F. Streffer, and J. Mayers, Phys. Rev. Lett. **79**, 2839 (1997).

[13] E. B. Karlsson, T. Abdul-Redah, R. M. F. Streffer, B. Hjörvarsson, J. Mayers, and C. A. Chatzidimitriou-Dreismann, Phys. Rev. B **67**, 184108 (2003).

[14] T. Abdul-Redah and C. A. Chatzidimitriou-Dreismann, Physica B **350**, E1035 (2004).

[15] C. A. Chatzidimitriou-Dreismann, T. Abdul-Redah, and J. Sperling, J. Chem. Phys. **113**, 2784 (2000).

[16] C. A. Chatzidimitriou-Dreismann, T. Abdul-Redah, R. M. F. Streffer, and J. Mayers, J. Chem. Phys. **116**, 1511 (2002).

[17] C. A. Chatzidimitriou-Dreismann, T. Abdul-Redah, and B. Kolaric, J. Am. Chem. Soc. **123**, 11945 (2001).

[18] C. A. Chatzidimitriou-Dreismann, T. Abdul-Redah, M. Krzystyniak, and M. Vos, in *Decoherence, Entanglement and Information Protection in Complex Quantum Systems*, edited by V. M. Akulin, A. Sarfati, G. Kurizki, and S. Pellegrin (Springer, Dordrecht, 2005), Vol. 483.

[19] M. Krzystyniak, T. Abdul-Redah, C. A. Chatzidimitriou-Dreismann, F. Filluax, E. B. Karlsson, J. Mayers, I. E. Mazets, H. Naumann, and S. Stenholm, in *Decoherence, Entanglement and Information Protection in Complex Quantum Systems*, edited by V. M. Akulin, A. Sarfati, G. Kurizki, and S. Pellegrin (Springer, Dordrecht, 2005), Vol. 439.

[20] T. Abdul-Redah, M. Krzystyniak, and C. A. Chatzidimitriou-Dreismann, in *Decoherence, Entanglement and Information Protection in Complex Quantum Systems*, edited by V. M. Akulin, A. Sarfati, G. Kurizki, and S. Pellegrin (Springer, Dordrecht, 2005), Vol. 469.

[21] R. A. Cowley, J. Phys.: Condens. Matter **15**, 4143 (2003).

[22] D. Colognesi, Physica B **344**, 73 (2004).

[23] H. Sugimoto, Aiko Okumura, and Hiroyuki Yuuki, Phys. Rev. B **73**, 014305 (2006).

[24] D. Colognesi, Physica B **398**, 89 (2007).

[25] S. E. McLain, C. J. Benmore, J. E. Siewenie, J. Urquidi, and J. F. C. Turner, Angew. Chem., Int. Ed. **43**, 1952 (2004).

[26] D. B. Northrop, Acc. Chem. Res. **34**, 790 (2001).

[27] T. D. B. Steiner, Angew. Chem., Int. Ed. **41**, 48 (2002).

[28] C. L. Perrin and J. B. Nielson, Annu. Rev. Phys. Chem. **48**, 511 (1997).

[29] M. W. Johnson, E. Sandor, and E. Arzi, Acta Crystallogr. B **31**, 1998 (1975).

[30] J. Janzen and L. S. Bartell, J. Chem. Phys. **50**, 3611 (1969).

[31] I. M. Mills, J. Phys. Chem. **88**, 532 (1984).

[32] G. C. Hancock and D. G. Truhlar, J. Chem. Phys. **90**, 3498 (1989).

[33] E. L. Sibert III, J. Phys. Chem. **93**, 5022 (1989).

[34] G. J. Fraser, J. Chem. Phys. **90**, 2097 (1989).

[35] A. S. Pine, W. J. Lafferty, and B. J. Howard, J. Chem. Phys. **81**, 2939 (1984).

[36] V. Garbuio, C. Andreani, S. Imberti, A. Pietropaolo, G. F. Reiter, R. Senesi, and M. A. Ricci, J. Chem. Phys. **127**, 154501 (2007).

[37] J. Mayers and T. Abdul-Redah, J. Phys.: Condens. Matter **16**, 4811 (2004).

[38] V. F. Sears, Phys. Rev. B **30**, 44 (1984).

[39] J. Mayers, C. Andreani, and G. Baciocco, Phys. Rev. B **39**, 2022 (1989).

[40] J. Mayers, Phys. Rev. B **41**, 41 (1990).

[41] J. Mayers, Phys. Rev. Lett. **71**, 1553 (1993).

[42] C. Andreani, D. Colognesi, and E. Pace, Phys. Rev. B **60**, 10008 (1999).

[43] G. B. West, Phys. Rep. **18**, 263 (1975).

[44] A. C. Evans, D. N. Timms, J. Mayers, and S. M. Bennington, Phys. Rev. B **53**, 3023 (1996).

[45] S. Imberti, C. Andreani, V. Garbuio, G. Gorini, A. Pietropaolo, R. Senesi, and M. Tardocchi, Nucl. Instrum. Methods Phys. Res. A **552**, 463 (2005).

[46] A. Pietropaolo, R. Senesi, C. Andreani, A. Botti, M. A. Ricci, and F. Bruni, Phys. Rev. Lett. **100**, 127802 (2008).

[47] H. Herzberg, *Molecular Spectra and Molecular Structure* (D. Van Nostrand, Princeton, NJ, 1945).

[48] G. B. Mitra and T. Chattopadhyay, Acta Crystallogr. A **28**, 179 (1972).

[49] H. Niu and M. Shimizu, J. Phys. Soc. Jpn. **22**, 437 (1967).

[50] V. F. Sears, Neutron News **3**, 26 (1992).

[51] H. R. Glyde, Phys. Rev. B **50**, 6726 (1994).

[52] M. Krzystyniak, C. A. Chatzidimitriou-Dreismann, M. Lerch, Z. T. Lalowicz, and A. Szymocha, J. Chem. Phys. **126**, 124501 (2007).

[53] G. F. Reiter, J. C. Li, J. Mayers, T. Abdul-Redah, and P. Platzman, Braz. J. Phys. **34**, 142 (2004).

[54] G. F. Reiter, J. Mayers, and T. Abdul-Redah, Physica B **385-386**, 234 (2006).

[55] G. Reiter, C. Burnham, D. Homouz, P. M. Platzman, J. Mayers, T. Abdul-Redah, A. P. Moravsky, J. C. Li, C.-K. Loong, and A. I. Kolesnikov, Phys. Rev. Lett. **97**, 247801 (2006).

[56] G. F. Reiter, J. Mayers, and J. Noreland, Phys. Rev. B **65**, 104305 (2002).

[57] Y. Qu, X. Bian, H. Tang, and P. Si, J. Mol. Struct.: THEOCHEM **671**, 173 (2004).

[58] G. M. Chaban and R. B. Gerber, Spectrochim. Acta, Part A **58**, 887 (2002).